

Article

# Using Isotopes (H, O, and Sr) and Major Ions to Identify Hydrogeochemical Characteristics of Groundwater in the Hongjiannao Lake Basin, Northwest China

Chu Wu, Xiong Wu \*, Wenping Mu and Ge Zhu

School of Water Resources and Environment, China University of Geosciences (Beijing), Beijing 100083, China; wuchu0613@cugb.edu.cn (C.W.); wuchu12345@163.com (W.M.); bently0613@126.com (G.Z.)

\* Correspondence: wuxiong@cugb.edu.cn

Received: 17 March 2020; Accepted: 19 May 2020; Published: 21 May 2020



**Abstract:** Hongjiannao Lake is the largest desert freshwater lake in the Ordos Plateau, China, and the relict gull is an endangered species that uses the lake for its habitat, with the largest colonies being located there. Using hydrochemical parameters, stable hydrogen and oxygen isotopes, and strontium isotopes, we investigated the hydrogeochemical characteristics of groundwater. As a result, the major cations of the groundwater were found to be  $\text{Ca}^{2+}$  and  $\text{Na}^+$ , the major anion was found to be  $\text{HCO}_3^-$ , and the hydrochemical facies were mainly found to be  $\text{HCO}_3\text{-Ca}$ ,  $\text{HCO}_3\text{-Na}$ . and  $\text{HCO}_3\text{-Ca-Na}$ . The hydrochemical formation of groundwater was controlled by both evaporation and water–rock interactions, and carbonate and sulfate minerals dissolved or precipitated in the groundwater. On the basis of isotope analysis, groundwater was affected by evaporation and  $\delta^{18}\text{O}$  enrichment, and the higher salinity of Hongjiannao Lake suffered from intensive evaporation. The higher  $^{87}\text{Sr}/^{86}\text{Sr}$  ratio and lower concentrations of  $\text{Sr}^{2+}$  in the groundwater were derived from the dissolution of silicate minerals, whereas the opposite concentrations were due to the dissolution of carbonate and sulfate minerals. Based on this work, such results can be used to research groundwater recharge into the lake and to protect water quality.

**Keywords:** isotope; hydrogeochemistry; groundwater flow; deuterium excess

## 1. Introduction

Water resources in China are unevenly distributed over space and time [1,2]. Northwest China is a region with severe drought and water shortage, and the protection and sustainable use of water resources is very important [3]. Moreover, groundwater plays a significant role in economic development in arid or semiarid areas [4], and it is necessary to first understand the hydrogeochemical characteristics and quality of groundwater [1,5]. The hydrochemical and isotopic method is one of the most common and effective approaches to identify the hydrogeochemical characteristics of groundwater. The chemical composition of groundwater is controlled by the composition and quantity of its rainfall, its geological structure, its aquifer minerals, and the hydrochemical evolution processes along its flow paths [6]. In combination with other data on geology, hydrology, and isotopes, information on groundwater hydrochemistry can be helpful in understanding the hydrogeochemical characteristics of groundwater [7,8]. In recent years, hydrochemistry and isotope approaches have become integral parts of the study of the hydrogeochemical characteristics of groundwater [9–12].

There are many lakes of varying sizes in the Ordos Plateau, Northwest China. Hongjiannao Lake (HL) is the largest desert freshwater lake in China, and seven seasonal rivers flow into it. The water filling HL can have many origins: Rainfall is a major source of water for HL, and other sources are

periodic overflows from rivers and groundwater discharge. The relict gull (*Larus relictus*) has been listed as an endangered species on the international union for conservation of nature (IUCN) Red List, and it uses the only island in HL as the habitat for its largest colonies [13]. In recent years, more severe human activity and climate warming have resulted in a continual decrease in the area of HL, and the water quality of HL has deteriorated [14]. Water shortages are becoming an increasing concern in the sustainable development of the Hongjiannao Lake area, which calls for the integrated and optimized management and utilization of groundwater and surface water resources. Liang and Yan (2017) investigated lake area variations and relict gull habitats by using Landsat imagery of Hongjiannao Lake [14]. Other studies have focused on the spatiotemporal changes in the water area and ecological environment in Hongjiannao Lake [13,15,16]. Moreover, many scholars have provided information on the origin, recharge mechanism, flow characteristics, and discharge behavior of groundwater in the Ordos Basin [17,18]. There is little research on hydrogeochemical characteristics on a local scale for the Hongjiannao Lake Basin, so we can better understand the processes that deliver chemicals to the lake by studying its groundwater chemistry, and it is necessary to conduct a detailed investigation of these aspects.

Moreover, hydrogeology studies can use the  $^{87}\text{Sr}/^{86}\text{Sr}$  ratio to determine water–rock interactions along the flow path and to identify dissolution and precipitation events. Liotta (2017) used the  $^{87}\text{Sr}/^{86}\text{Sr}$  ratio to trace the groundwater flow in the volcanic edifice of Mt. Etna [19]. Similarly, other scholars have calculated the  $^{87}\text{Sr}/^{86}\text{Sr}$  ratio and used other isotopes and hydrochemical characteristics to investigate groundwater flow and characterization in some areas [20–23]. According to an analysis of the Sr concentration and the  $^{87}\text{Sr}/^{86}\text{Sr}$  ratio in an aquifer matrix of the Cretaceous Basin, Ordos Plateau, Su (2011) revealed that silicate minerals have a lower Sr concentration and a higher  $^{87}\text{Sr}/^{86}\text{Sr}$  ratio, and carbonate and sulfate minerals have the opposite properties [24]; here, many of the ion concentrations and the  $^{87}\text{Sr}/^{86}\text{Sr}$  ratio were found to be dependent on the interaction of the groundwater with the aquifer matrix [25]. Hence, spatial variations in the chemistry of groundwater and the  $^{87}\text{Sr}/^{86}\text{Sr}$  ratio can be useful in elucidating the hydrogeochemical characteristics of groundwater.

In the study area, knowledge of the hydrogeochemical characteristics of groundwater is a key issue for the sustainable use of water resources and for mitigating the deterioration of the ecological environment. Given this, using hydrochemical parameters, hydrogen and oxygen isotopes, and Sr isotopes, we investigated the hydrogeochemical characteristics and their changes along the groundwater flow path of Hongjiannao Lake according to south–north and west–east profiles. Based on the hydrogeochemical characteristics of groundwater, we could evaluate the groundwater quality for the sustainable use of water resources, and we could establish a numerical model of groundwater to study groundwater discharge into the lake.

## 2. Description of the Study Area

### 2.1. Study Location and Climate

The study area (Hongjiannao Basin) comprises Hongjiannao Lake (HL) and many seasonal rivers; all rivers and groundwater drain into HL. HL is a young inland lake and the largest desert freshwater lake in China. Hongjiannao Basin (HB) is located in the mid-north region of the Ordos Basin and in the south of Ordos City, Inner Mongolia Autonomous Region (Figure 1), and it constitutes a surface area of approximately 1440 km<sup>2</sup>. HL is the largest desert freshwater lake in China with a water surface area of approximately 35 km<sup>2</sup>, and its maximum depth is approximately 7 m. It is located at the eastern edge of the Maowusu desert and belongs to both Inner Mongolia and Shaanxi Province. HB has an arid or semiarid temperate plateau continental climate with low rainfall and high evaporation. The average annual rainfall is 359.6 mm, and the annual rainfall is concentrated between July and September, which accounts for 69% of the total annual rainfall [14]. The average annual evaporation of 2485.2 mm is approximately seven times the average annual rainfall. The region is dominated by

western and northwestern trade winds with an average annual velocity of 3.4 m/s, and the average annual temperature is 8.5 °C [16].

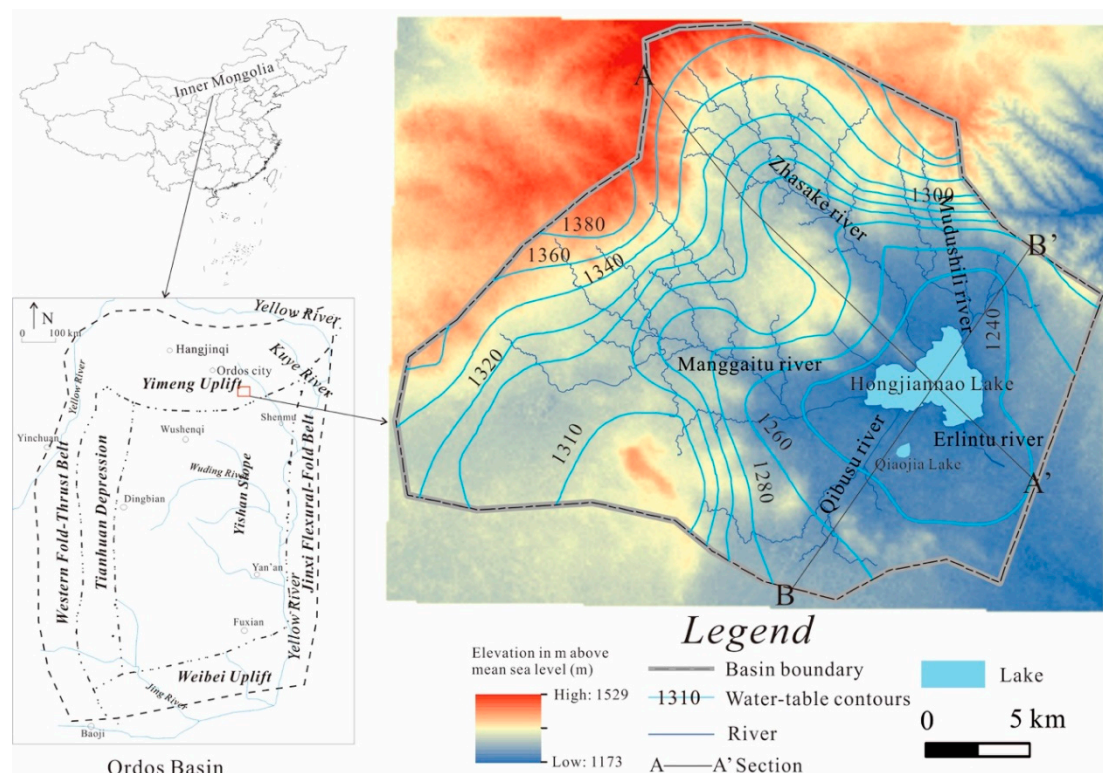


**Figure 1.** Location and hydrogeological condition of the study area.

## 2.2. Hydrological, Geological and Hydrogeological Setting

Five rivers flow into HL (Figure 1). The Zhasake River, the Manggaitu River, and the Mudushili River are affiliated with Inner Mongolia, and inflows from these rivers account for approximately 63% of the river water flowing into the lake. The other two rivers, the Qibusu River and the Erlintu River, are located in Shaanxi Province [16]. In terms of the regional geology, the area belongs to the Yimeng uplift of the Ordos platform syncline and is located in the eastern region of the Yimeng uplift. The local watershed comprises three major geological time slices: the Jurassic, Cretaceous, and Quaternary periods.

The Quaternary lacustrine-pluvial deposit mainly consists of sand gravel and medium-coarse sand with a thin layer of clayey sand, a diluvial-pluvial deposit of fine sand, silt, sandy clay, medium-coarse sand, and an eolian deposit of fine sand that constitutes the Quaternary aquifer (Figure 2). The distribution of the Quaternary aquifer is variable, and the thickness varies greatly from 1 to 30 m. The depth of the groundwater is dominated by the terrain. The Luohe Formation of the Cretaceous aquifer is overlain by desert sediments and fluvial sediments, which consist of quartz sandstone and arkose sandstone, occasionally with thin mudstone and local gypsum. The Huanhe Formation of the Cretaceous aquifer is dominated by fluvial sediments that comprise arkose sandstone and pebbly sandstone, occasionally with thin mudstone and argillaceous siltstone. The Cretaceous aquifer of the Luohe and Huanhe Formations have close hydraulic connections with the overlying Quaternary aquifer. The thickness of the Cretaceous sediments gradually decreases from east to west until encountering the underlying Jurassic sediments, which consist of mudstone, sand mudstone, and coal, as a relative aquiclude. In terms of the terrain topography, HL is located in low-lying terrain, and the HB boundary with higher terrain can be regarded as a local watershed. Quaternary groundwater runs off with the terrain draining into HL, and Cretaceous groundwater basically dominates horizontal flow from east to west, encountering the Jurassic aquiclude and draining into HL.

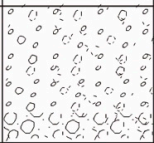
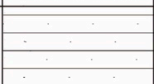
System	Stage	Thick-ness (m)	Column	Stratum feature
Quaternary	Q <sub>4</sub>	0-25		Lacustrine-pluvial: sand gravel and medium-coarse sand Diluvial-pluvial: fine sand, silt, sandy clay and medium-coarse sand Eolian: fine sand
Cretaceous	Luohe(K <sub>1</sub> l)	40-230		quartz sandstone and arkose sandstone, occasionally with thin mudstone and local gypsum
	Huanhe(K <sub>1</sub> h)	30-80		arkose sandstone and pebbly sandstone occasionally with thin mudstone and argillaceous siltstone
Jurassic	Anding(J <sub>2</sub> a)	10-80		mudstone, sandy mudstone
	Zhiluo(J <sub>2</sub> z)	1-278		mudstone, sandy mudstone and 1 <sup>th</sup> coal seam
	Yanan(J <sub>2</sub> y)	78-247		sandy mudstone, mudstone and 2 <sup>th</sup> , 3 <sup>th</sup> , 4 <sup>th</sup> , 5 <sup>th</sup> , 6 <sup>th</sup> , 7 <sup>th</sup> coal seam

Figure 2. Stratigraphic column of the study area.

### 3. Data and Methods

#### 3.1. Sample Collection and Analysis

In the study area, groundwater samples were collected from hand-pumped tube wells and motor-pumped wells, lake water samples were taken from 1–2 m below the water surface by a hand-held peristaltic pump, and lake-bottom sediments were taken from 0.5 m below the sludge deposits by a piston-column bottom sampler (TC-600H) in August 2018. Groundwater and lake water samples were filtered through 0.45 µm membrane filters and collected in clean and dry polyethylene plastic bottles after pumping until the flowing water showed stabilized temperature, pH, dissolved O<sub>2</sub>, and

Eh values. The water samples used for the major element and strontium isotope analysis were collected in 100 mL HNO<sub>3</sub> washed polyethylene plastic bottles, followed by the addition of 6 M HNO<sub>3</sub> to obtain a pH < 2. Sample collection, handling, and storage followed the standard procedures recommended by the Chinese Ministry of Water Resources. Meanwhile, field-based water parameters, such as temperature, pH, and electric conductivity (EC), were measured in situ with a multi-parameter portable meter (HANNA, HI9828). HCO<sub>3</sub><sup>3-</sup> was titrated in the field using a portable testing kit produced by Merck KGaA Co. (Germany). Chemical and isotope analyses of water samples and sediment samples were performed at the Nuclear Industrial Geology Analysis and Testing Research Center, Beijing, China. Unfiltered samples for the stable water isotope (δD and δ<sup>18</sup>O) analyses were collected in 50 mL High Density Polyethylene (HDPE) bottles and sealed with Polyethylene (PE) caps. The dissolved concentrations of major anions (Cl<sup>-</sup>, NO<sub>3</sub><sup>-</sup>, and SO<sub>4</sub><sup>2-</sup>) and cations (Ca<sup>2+</sup>, Mg<sup>2+</sup>, K<sup>+</sup>, and Na<sup>+</sup>) were analyzed by means of ion chromatography (ICS-1100 systems). The strontium concentrations were measured using inductively coupled plasma–mass spectrometry (ICP–MS, NexION300D), calibrated with a multi-element standard. The relative standard deviation for the replicates of all major ions and strontium concentrations analyses was within ± 5%. <sup>87</sup>Sr and <sup>86</sup>Sr were measured using a Finnigan MAT-253 multiple collector thermal ionization mass spectrometer (TIMS). All reported values of the <sup>87</sup>Sr/<sup>86</sup>Sr ratios were normalized for fractionation to <sup>87</sup>Sr/<sup>86</sup>Sr = 0.1194, and the measured value of the NIST\_NBS 987 (SrCO<sub>3</sub>) standard was 0.710242 ± 0.000012 (2σ, n = 16). The stable isotopes (δD and δ<sup>18</sup>O) were measured using a Delta and XP isotope ratio mass spectrometer (IRMS). The isotopic composition of oxygen and hydrogen are reported in the usual δ-scale in parts per thousand [26]:

$$\delta_{\text{sample}}(\text{‰}) = \frac{R_{\text{sample}} - R_{\text{standard}}}{R_{\text{standard}}} \times 100 \quad (1)$$

where R is D/H, or the  $^{18}\text{O}/^{16}\text{O}$  abundance ratio. Reported values were corrected on the VSMOW2/SLAP2 scale. Repeated analyses of in-house reference water showed a precision better than  $\pm 0.1\text{‰}$  for  $^{18}\text{O}/^{16}\text{O}$  and  $\pm 1.0\text{‰}$  for D/H.

### 3.2. Methods

The saturation index (SI) is used to describe the equilibrium state of water with respect to mineral phases and to determine the dissolution or precipitation of minerals in rock–water interactions [1,5,6]. This index was calculated by using Equation (2):

$$\text{SI} = \log\left(\frac{\text{IAP}}{\text{K}_s}\right) \quad (2)$$

where IAP is the ion activity product of the solution and  $\text{K}_s$  is the solubility product of the mineral.  $\text{SI} = 0$  indicates equilibrium,  $\text{SI} > 0$  indicates oversaturation (precipitation), and  $\text{SI} < 0$  indicates undersaturation (dissolution).

Based on the previous research results and stratum feature in the study area, we calculated the SIs of calcite, dolomite, and gypsum by using the hydrochemical parameters of groundwater. According to the change of SIs along the groundwater flow path, we investigated the dissolution or precipitation of minerals and water–rock interactions.

The cation exchange was confirmed by chloro-alkaline CAI-1 [1,27], and the index was usually calculated using the following formula:

$$\text{CAI} - 1 = \frac{\text{Cl}^- - (\text{Na}^+ + \text{K}^+)}{\text{Cl}^-} \quad (3)$$

If the index was greater than zero, this indicated the exchange of  $\text{Na}^+$  and/or  $\text{K}^+$  in the groundwater with  $\text{Mg}^{2+}$  and/or  $\text{Ca}^{2+}$  in aquifer materials. If the index was negative, then the cation exchange occurred in the reverse order. Furthermore, if the absolute values of the index were greater, a stronger cation exchange occurred in the groundwater environment.

In the study area, we investigated hydrochemical characteristics by the change of CAI-1 along the groundwater flow path. Moreover, we calculated the hydrochemical facies of groundwater by using the AQQA software. The change of hydrochemical facies along the groundwater flow path better explained the hydrogeochemical characteristics of the groundwater.

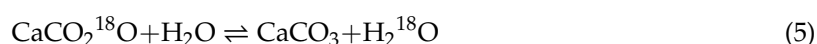
Dansgaard (1964) proposed that the surplus of deuterium relative to the global meteoric water line (GWML, slope = 8) can be denoted by d, also known as the d-index (Equation (4)), and can apparently be used for indicating nonequilibrium conditions [26].

$$d = \delta\text{D} - 8 \times \delta^{18}\text{O} \quad (4)$$

The d-index can reflect the imbalance of the degree of evaporation intensity and the condensation process of rainfall [28].

Moreover, isotope exchange was accompanied by water–rock interactions in the groundwater environment. The isotope exchange did not significantly affect the  $\delta\text{D}$  value of the groundwater, and the oxygen isotope exchange caused  $\delta^{18}\text{O}$  enrichment; the d-index had a tendency to decrease in the groundwater environment [29]. There are several kinds of isotope exchange reactions [30], such as those shown in Equations (5)–(7).

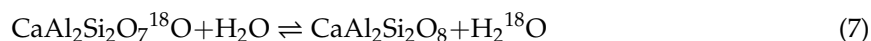
The  $^{18}\text{O}$  exchange between water and calcite:



The  $^{18}\text{O}$  exchange between water and quartz:



The  $^{18}\text{O}$  exchange between water and anorthite:



In the groundwater environment, stronger water–rock interactions were accompanied greater isotope exchange, making the d-index smaller. In other words, the value of the d-index could be used to indicate the degree of isotope exchange between water and rock. The smaller d-index of groundwater or the greater difference in the d-index between that of groundwater and that of the recharge area suggested that the groundwater flow path rate was slow and that its stagnation time was long and may have been affected by evaporation [31].

## 4. Results and Discussion

### 4.1. Hydrochemical Characterization

As shown in Table A1, the groundwater had a concentration of  $\text{Na}^+$  ranging from 10.10 to 152.00 mg/L, and the mean concentration of  $\text{Na}^+$  was 58.05 mg/L. In general,  $\text{Cl}^-$  and  $\text{Na}^+$  had a strong correlation in the groundwater environment; the mean concentration of  $\text{Cl}^-$  was 25.71 mg/L, which was smaller than that of  $\text{Na}^+$ , and may have been due to the cation exchange [1,5]. In the study area, calcite and dolomite were common carbonate minerals.  $\text{Ca}^{2+}$ ,  $\text{Mg}^{2+}$ , and  $\text{HCO}_3^-$  in the groundwater mainly came from the dissolution of carbonate minerals; the mean  $\text{Ca}^{2+}$  concentration of 53.08 mg/L was higher than that of  $\text{Mg}^{2+}$  (14.70 mg/L), and the mean concentration of  $\text{HCO}_3^-$  was 260.67 mg/L. The aquifer matrix contained gypsum locally, the excess  $\text{Ca}^{2+}$  may have come from the dissolution of gypsum, and the mean  $\text{SO}_4^{2-}$  concentration of 53.08 mg/L was less than that of  $\text{Ca}^{2+}$ . In general, the major cations for the groundwater were  $\text{Ca}^{2+}$  and  $\text{Na}^+$ , and the major anion was  $\text{HCO}_3^-$  in the study area. The hydrochemical facies of the groundwater were calculated by the AQQA software, as shown in Table 1. The dominant hydrochemical facies of groundwater were found to be the  $\text{HCO}_3\text{-Ca-Na}$ ,  $\text{HCO}_3\text{-Ca}$ , and  $\text{HCO}_3\text{-Na}$  types in the study area. Then, we analyzed the hydrogeochemical characteristics of the groundwater along the south–north and west–east profiles.

**Table 1.** Calculated results of hydrochemical type, saturation index, CAI-1 (chloro-alkaline) and d-index (surplus of deuterium relative to the GWML) (sample locations shown in Figure 3).

Sample	Hydrochemical Type	Saturation Index			CAI-1	d-Index (‰)
		Calcite	Gypsum	Dolomite		
D46	$\text{HCO}_3\text{-Ca}$	0.11	−2.32	−0.1	−1.46	3.5
D15	$\text{HCO}_3\text{-Ca}$	0.74	−1.89	1.49	−0.59	3.3
D04	$\text{HCO}_3\text{-Ca}$	0.63	−2.31	0.93	−1.34	3.9
D12	$\text{HCO}_3\text{-Ca}$	0.31	−1.74	0.13	−1.53	−0.6
D23	$\text{HCO}_3\text{-Ca}$	0.37	−1.82	0.65	0.35	4.2
D20	$\text{HCO}_3\text{-Ca-Na}$	0.14	−2.66	0.04	−5.86	−10
D37	$\text{HCO}_3\text{-Ca}$	0.86	−2.99	1.5	−1.34	0.8
D55	$\text{HCO}_3\text{-Ca}$	0.53	−2.37	0.99	−0.27	−8.6
D42	$\text{HCO}_3\text{-Ca-Na}$	0.05	−3.06	−0.1	−1.61	−0.5
D26	$\text{HCO}_3\text{-Ca-Na}$	0.39	−2.24	0.57	−1.68	−2.7
D09	$\text{HCO}_3\text{-Na}$	0.06	−2.7	0.19	−3.22	−4.5
D01	$\text{HCO}_3\text{-Ca}$	0.76	−1.67	1.1	−1.74	−3.7

### 4.2. TDS Concentration Variations

Section A–A' starts at the upper reaches of the Zhasake River and extends to the upper reaches of the Eelintu River with a total length of approximately 37 km (Figure 3a). In terms of the terrain

topography, the terrain is slightly undulating along the section from 1475 to 1230 m until 1249 m, and the HL level is the lowest. The thickness of the Quaternary aquifer in the western part of HL is uniform with an average of 7 m. Section B–B’ starts at the upper reaches of the Qibusu River and extends to the northern mountain region with a total length of 31 km (Figure 3b). It has flat terrain with an elevation from 1276 to 1265 m. On both sides of the section, the thickness of the Quaternary strata is uniform at approximately 27 m, and the thickness of the Cretaceous sandstone is thin with an average thickness of 15 m. The Quaternary aquifer south of the lake mainly consists of lacustrine-pluvial and diluvial-pluvial sand, and the groundwater depth is shallow at 1–2 m.

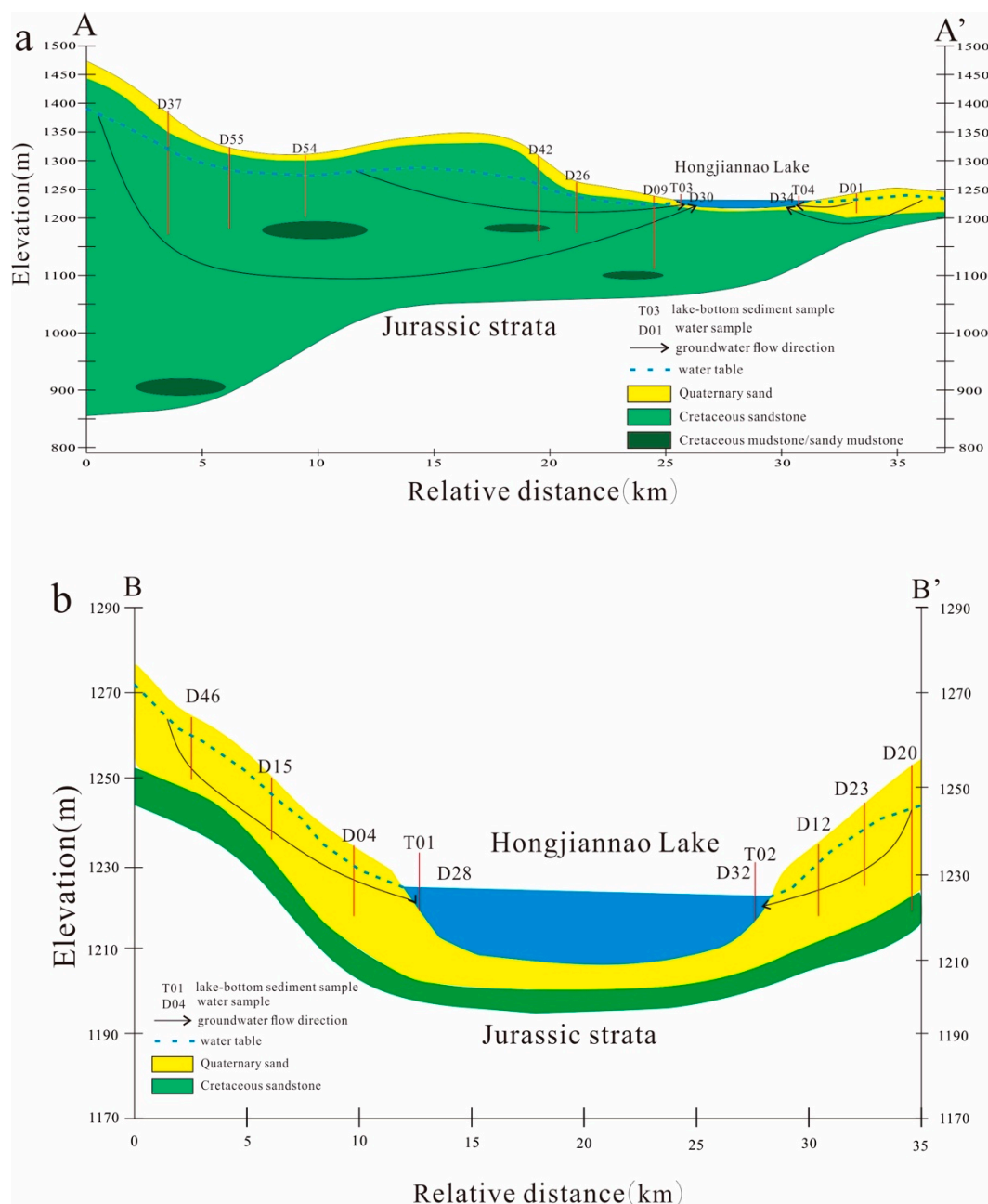


**Figure 3.** Hydrogeologic profile of the A–A’ (a) and B–B’ (b) and sampling locations (refer to Figure 1 for locations in the caption).

Table A1 shows the hydrochemical parameters and isotopes (H, O, and Sr) of the water samples. There were six groundwater samples and two lake water samples from section A–A’. Among the

five groundwater samples taken from Cretaceous pore-fissure water, the total dissolved solids (TDS) concentration began to increase and then decrease along the groundwater flow path northwest of HL (Figure 4a). The lake water had a TDS concentration of approximately 7.0 g/L due to strong evaporation [32,33]. Moreover, the Quaternary pore water (D01) east of HL with a depth of approximately 3.11 m had a TDS concentration of 536 mg/L, which was greater than that of the Cretaceous pore-fissure water.

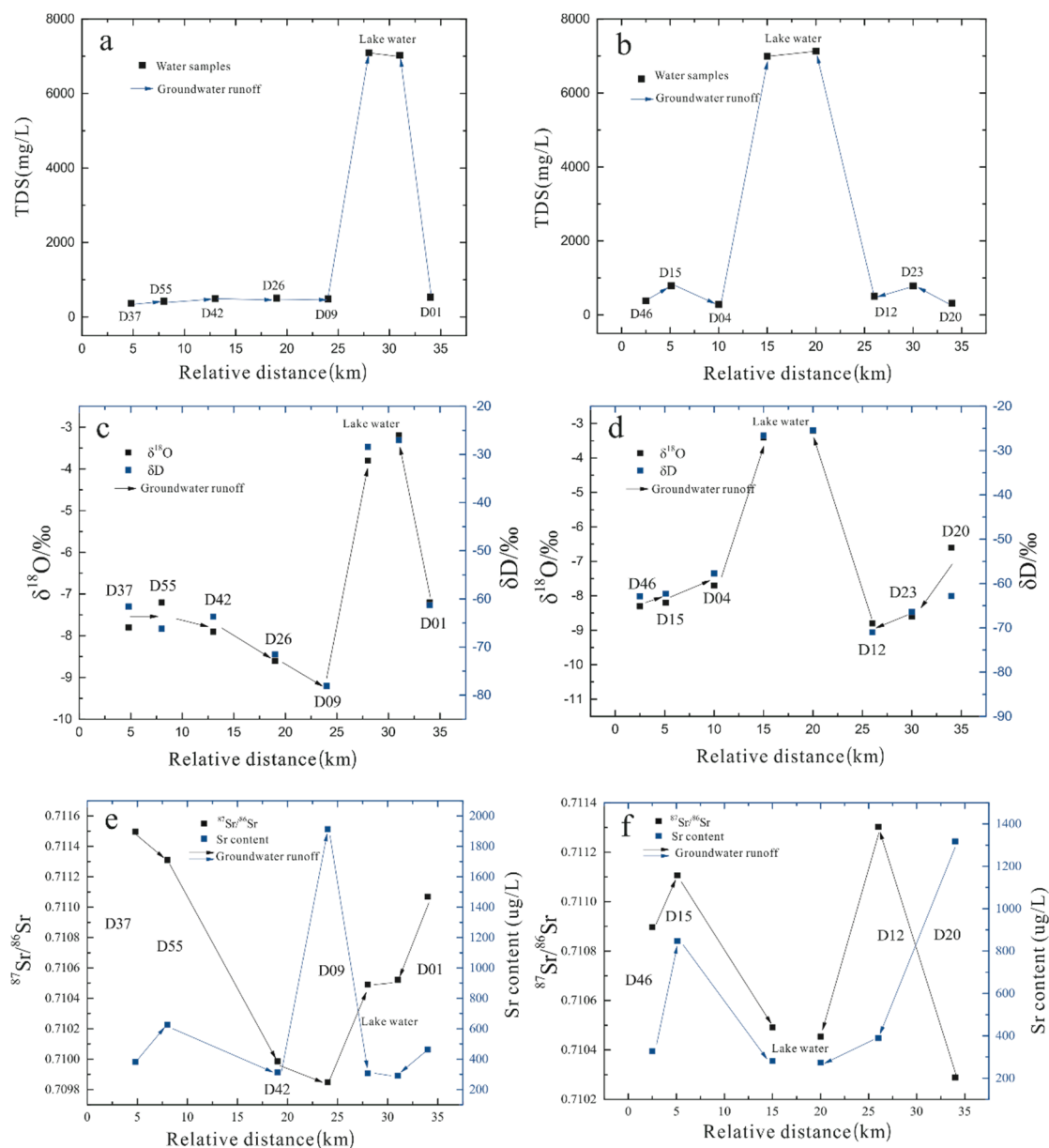


**Figure 4.** Change in TDS concentrations and isotopes (H, O, and Sr) along the groundwater flow path (a, c, and e for section A–A', b, d, and f for section B–B').

For section B–B', five groundwater samples were taken from the Quaternary aquifer, and one (D20) was taken from the Cretaceous aquifer. As shown in Figure 4b, the TDS concentration began to increase and then decrease along the groundwater flow path on both sides of the section until reaching the lake, and the TDS concentration in the lake water sample was up to 7.0 g/L. The D15 groundwater sample was from a location north of Qiaojia Lake (reedy marshes), and the groundwater depth was 1.36 m. The TDS concentration in phreatic water varied spatially, and was closely related

with the strong evaporation conditions in the Northwest, China [32]. The TDS concentration of D15 was 787 mg/L, which may have been due to both groundwater recharge by the surface water of Qiaojia Lake and strong evaporation. Moreover, the groundwater (D23) depth was shallow at 2.85 m, which may have been due to evaporation, which resulted in a TDS concentration of up to 782 mg/L [4,32].

Both sections showed consistent changes in TDS concentration, except for the D01 groundwater sample. At both ends of the sections, groundwater was mainly recharged by rainfall with lower TDS concentrations. TDS concentrations began to increase and then decrease along the groundwater flow path. Closest to the lakeshore, groundwater became fresher because of mixing due to the convergence of flows from Cretaceous groundwater flow paths.

#### 4.3. Hydrochemical Variations along Groundwater Flow Path

The major cations for the groundwater were  $\text{Ca}^{2+}$  and  $\text{Na}^+$ , and the major anion was  $\text{HCO}_3^-$  in section B–B'. For the southern portion of section B–B', the dominant hydrochemical facies of the Quaternary groundwater was the  $\text{HCO}_3\text{--Ca}$  type, and gypsum was in a dissolution state; in contrast, calcite and dolomite generally tended to precipitate (Table 1). The three SIs of sample D15 were greater than those of D46 and D04, and CAI-1 was smaller. When combined with the results in the chapter of TDS concentration variation, it can be observed that D15 sample had a weaker water–rock interaction and stronger evaporation than the other two samples [4,5]. As shown in Table 1, the dominant hydrochemical facies of the samples from the northern portion of section B–B' were the  $\text{HCO}_3\text{--Ca--Na}$ ,  $\text{HCO}_3\text{--Ca}$ , and  $\text{HCO}_3\text{--Na}$  types, and the SI of minerals was similar to that from the southern portion of section B–B'. The  $\text{Ca}^{2+}$  was mainly derived from the dissolution of gypsum, the CAI-1 of the D20 sample was  $-5.86$ , and a stronger cation exchange occurred between the dissolved  $\text{Ca}^{2+}$  in the groundwater and the absorbed  $\text{Na}^+$  on the surface of the clay minerals that released abundant  $\text{Na}^+$  into the groundwater. This result was consistent with the analysis of stable isotopes, which indicated that the D20 sample had a stronger water–rock interaction than the other samples.

Meanwhile, groundwater flow to the D23 sample indicated that calcite and dolomite had a stronger oversaturation and that the undersaturation of gypsum was weaker than at the other sampling locations. The CAI-1 of the D23 sample was positive, indicating that the dissolved  $\text{Na}^+$  in the groundwater exchanged absorbed  $\text{Ca}^{2+}$ , and then the  $\text{Na}^+$  concentration decreased. The hydrochemical facies changed from the  $\text{HCO}_3\text{--Ca--Na}$  type to the  $\text{HCO}_3\text{--Ca}$  type, also suggesting that groundwater flow near the D23 sampling point was rapid and that it had weaker water–rock interactions. The hydrochemical facies of the D12 sample near the discharge area was of the  $\text{HCO}_3\text{--Ca}$  type, the SI values slightly increased, and the cation exchange changed direction, which revealed stronger water–rock interactions and a slower groundwater flow in the groundwater environment compared to that at the other sampling locations.

The major cations in the groundwater were  $\text{Ca}^{2+}$  and  $\text{Na}^+$ , and the major anion was  $\text{HCO}_3^-$  in section A–A'. As shown in Table 1, in the western portion of section A–A', the hydrochemical facies of the groundwater samples were the  $\text{HCO}_3\text{--Ca}$ ,  $\text{HCO}_3\text{--Ca--Na}$ , and  $\text{HCO}_3\text{--Na}$  types, and the  $\text{Na}^+$  gradually replaced the  $\text{Ca}^{2+}$  along the groundwater flow path. The D37 sample was located in the upper reach of the Zhasake River, and the groundwater was mainly recharged by rainfall. From D37 to D55, the SI values of calcite and dolomite slightly decreased, and the dissolution of gypsum and the cation exchange became weaker, suggesting weaker water–rock interactions. In the groundwater flow area, gypsum in the D42 sample was in a dissolution state, and the dissolved state of calcite and dolomite tended towards equilibration. Meanwhile, a stronger cation exchange occurred between the dissolved  $\text{Ca}^{2+}$  in the groundwater, and  $\text{Na}^+$  was absorbed on the surface of the clay minerals; the hydrochemical facies was the  $\text{HCO}_3\text{--Ca--Na}$  type. In the D26 sample, the cation exchange was basically unchanged, the SI values increased, and the hydrochemical facies was also of the  $\text{HCO}_3\text{--Ca--Na}$  type. Near the discharge area, the SI values for calcite and dolomite were close to zero, the dissolved  $\text{Ca}^{2+}$  in the groundwater positively exchanged absorbed  $\text{Na}^+$ , and the hydrochemical facies of the D09 sample was the  $\text{HCO}_3\text{--Na}$  type.

As a whole, the major cations in the groundwater were  $\text{Ca}^{2+}$  and  $\text{Na}^+$ , the major anion was  $\text{HCO}_3^-$ , and the hydrochemical facies changed cations along the groundwater flow path. The gypsum was actively dissolved in the groundwater; however, calcite and dolomite tended to precipitate, and hydrochemical formation was mainly influenced by both water–rock interactions and evaporation [1,5].

#### 4.4. Stable Water Isotopes ( $\delta\text{D}$ and $\delta^{18}\text{O}$ )

As shown in Figure 5, groundwater samples were located at the right of the global meteoric water line (GMWL,  $\delta\text{D} = 8\delta^{18}\text{O} + 10$ ) and local meteoric water line (LMWL,  $\delta\text{D} = 6.4\delta^{18}\text{O} - 4.07$ ) from Baotou, Inner Mongolia, China, and the lake samples basically fell on the LMWL [33]. In the study area, all water samples were located near the GMWL and LMWL. Evaporative enrichment at the open water surface is created by the enrichment of the heavier isotopes [34]. The lake water samples fell into the LMWL, indicating that the lake water was mainly recharged by atmospheric rainfall, and it had heavier isotopes, because open water is affected by intensive evaporation [6,35]. The groundwater samples plotted in the lower right from the GMWL and LMWL, indicating that groundwater was of a meteoric origin and a “ $\delta^{18}\text{O}$  shift” to a differing extent took place. as did a relatively strong water–rock interaction. This can be explained by an isotope exchange reaction [4,6,7,36].

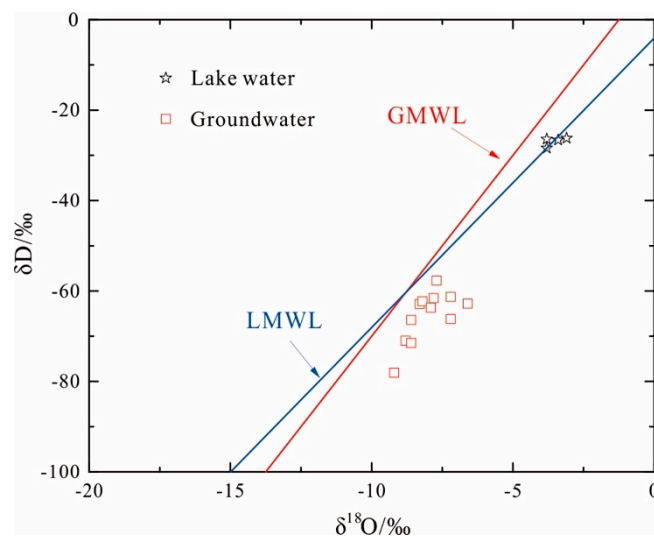


**Figure 5.** Plot of  $\delta\text{D}$  and  $\delta^{18}\text{O}$  of groundwater and lake water.

As shown in Figure 4c, the stable isotope values ( $\delta^{18}\text{O}$  and  $\delta\text{D}$ ) of the groundwater from the Cretaceous aquifer gradually decreased along the groundwater flow path from section A–A', and the difference value of  $\delta^{18}\text{O}$  was positively correlated with the distance between sampling points. The groundwater sample D37 was located in the regional watershed with the lowest  $\delta^{18}\text{O}$  value, which had an obvious and significant influence on the groundwater. The d-index of sample D55 was  $-8.6\text{‰}$  (Table 1), with a groundwater depth of approximately 6 m, suggesting that this area has stronger water–rock interactions and a slower groundwater flow rate.

On the other hand, the stable isotope values of the Quaternary groundwater gradually increased along the groundwater flow path in the south region of section B–B' (Figure 4d). The groundwater sample D46 was located in the upper reach of the QPR, where the groundwater was mainly recharged by rainfall, and its stable isotopes were close to those for rainfall. The average d-index was  $2.86\text{‰}$ , which indicated a rapid groundwater flow rate, and the  $\delta^{18}\text{O}$  and  $\delta\text{D}$  were gradually enriched, mainly due to evaporation. The situation in the north region of section B–B' was opposite to that of the south, and the  $\delta^{18}\text{O}$  and  $\delta\text{D}$  of the groundwater gradually decreased along the groundwater flow path. In sample D20, taken from the Cretaceous aquifer with a groundwater depth of 19.4 m and a d-index of  $-10\text{‰}$ , the lateral recharge of the northern mountain area had a stronger water–rock interaction.

Moreover, the d-indexes of samples D23 and D12 were 4.2‰ and −0.6‰, respectively, with shallower groundwater depths, suggesting that the groundwater chemistry was affected by both evaporation and water–rock interactions [33,34].

#### 4.5. Sr Concentration and Sr Isotopic Characterization

##### 4.5.1. Sr Isotope and Concentrations

Studies applying strontium isotopes have been used to determine the sources of solutes in groundwater [37,38], to understand the hydrochemical evolution of groundwater [39,40], and to quantify the contributions of different sources of groundwater [41,42]. Differences in  $^{87}\text{Sr}/^{86}\text{Sr}$  ratios between the different aquifers and between the ratios in an aquiferous medium and the ratios in rainfall make strontium an ideal tracer for identifying groundwater flow paths and water–rock interactions, as well as for studying the influence of rainfall on groundwater recharge [43]. Based on previous studies of strontium isotopes for Cretaceous groundwater in the Ordos Basin [24,44], a mineral analysis by X-ray diffraction revealed that the matrixes of aquifers mainly consisted of quartz, K-feldspar, albite, calcite, dolomite, illite, and chlorite, and a gypsum-bearing layer was often found in aquifers as evidence of the presence of gypsum minerals. Moreover, Su (2011) analyzed the strontium concentrations and the  $^{87}\text{Sr}/^{86}\text{Sr}$  ratio of minerals in the matrix of aquifers, suggesting lower strontium concentrations and higher  $^{87}\text{Sr}/^{86}\text{Sr}$  ratios in the silicate minerals; however, carbonate and sulfate minerals were found to have the opposite characteristics [24].

In section A–A', the strontium concentrations of the five groundwater samples ranged from 314 to 1941  $\mu\text{g}/\text{L}$ , and the  $^{87}\text{Sr}/^{86}\text{Sr}$  ratio ranged from 0.709848 to 0.711498 (Table A1). The strontium concentrations of the D09 sample was 1941  $\mu\text{g}/\text{L}$ , and its  $^{87}\text{Sr}/^{86}\text{Sr}$  ratio was 0.709848, suggesting that the source of strontium was mainly derived from the weathering dissolution of carbonate and sulfate minerals in the groundwater environment. The higher strontium concentration may have been affected by the Jurassic strata. The D37 sample had a higher  $^{87}\text{Sr}/^{86}\text{Sr}$  ratio and lower strontium concentrations, which may have been due to the silicate minerals dissolved in the groundwater. Moreover, the higher  $^{87}\text{Sr}/^{86}\text{Sr}$  ratio was close to that of rainfall, indicating that the groundwater was mainly recharged by rainfall. Combined with the sampling position, this situation was in agreement with the hydrogeological survey. As shown in Figure 4e, the  $^{87}\text{Sr}/^{86}\text{Sr}$  ratio gradually decreased along the groundwater flow path because the dissolution of carbonate and sulfate minerals could have released a lower  $^{87}\text{Sr}/^{86}\text{Sr}$  ratio and higher strontium concentrations into the groundwater, causing the strontium concentrations of D55 and D09 to increase.

As shown in Table A1, the strontium concentrations and the  $^{87}\text{Sr}/^{86}\text{Sr}$  ratio were basically unchanged in both lake samples, and the  $^{87}\text{Sr}/^{86}\text{Sr}$  ratio was close to the lower limit of rainfall (0.71097~0.711682), suggesting that the lake water mainly recharged by rainfall. The T03 and T04 samples were taken from lake-bottom sediments, where the strontium concentrations were found to be 450 and 225  $\mu\text{g}/\text{L}$ , respectively, and the  $^{87}\text{Sr}/^{86}\text{Sr}$  ratios were found to be 0.712705 and 0.715187, respectively (Table 2). These values were all greater than those of the near groundwater samples, indicating that lake-bottom sediments containing Sr minerals were less likely to dissolve into the lake.

**Table 2.** Strontium isotope and concentrations of lake-bottom sediments and minerals.

Sample	$\text{Sr}^{2+}$ ( $\mu\text{g}/\text{g}$ )	$^{87}\text{Sr}/^{86}\text{Sr}$
T01	282	0.713994
T02	530	0.712538
T03	225	0.715187
T04	450	0.712705
Silicate minerals weathering		0.716–0.720
Carbonate minerals weathering		0.708

Similarly, the strontium concentrations and the  $^{87}\text{Sr}/^{86}\text{Sr}$  ratios of the groundwater samples ranged from 327 to 1318  $\mu\text{g}/\text{L}$  and from 0.710288 to 0.711303, respectively, in section B–B'. The strontium concentrations and the  $^{87}\text{Sr}/^{86}\text{Sr}$  ratio of the D20 sample were 1318 and 0.710288  $\mu\text{g}/\text{L}$ , respectively. Moreover, the D20 and D12 samples were taken from the groundwater runoff area, and the strontium concentrations and the  $^{87}\text{Sr}/^{86}\text{Sr}$  ratio were affected by mineral dissolution in the water–rock interactions. The results of the stable isotope ( $\delta^{18}\text{O}$  and  $\delta\text{D}$ ) analysis revealed that groundwater (D46) was mainly recharged by rainfall, and its  $^{87}\text{Sr}/^{86}\text{Sr}$  ratio was close to the lower limit of rainfall. As shown in Figure 4f, the strontium concentrations and the  $^{87}\text{Sr}/^{86}\text{Sr}$  ratios increased from D46 to D15. Groundwater (D15) with a shallow depth may have been recharged by Qiaojia Lake, and its  $^{87}\text{Sr}/^{86}\text{Sr}$  ratio approached the upper limit of rainfall, suggesting that the groundwater was mainly recharged by rainfall and that the higher strontium concentrations may have been due to the dissolution of carbonate and sulfate minerals. As a whole, the D46, D15, and D12 samples in section B–B' were all taken from shallow groundwater, and their  $^{87}\text{Sr}/^{86}\text{Sr}$  ratios were close to that of rainfall, indicating that shallow groundwater was mainly recharged by rainfall; the change in strontium concentrations was affected by the dissolution of different minerals in the water–rock interactions. The relationship between the  $^{87}\text{Sr}/^{86}\text{Sr}$  ratio and  $\delta^{18}\text{O}$  provided an additional test of the regional flow hypothesis [45]. As shown in Figure 6, the  $^{87}\text{Sr}/^{86}\text{Sr}$  ratio had positive relationship with  $\delta^{18}\text{O}$  as a whole. The  $^{87}\text{Sr}/^{86}\text{Sr}$  ratio of groundwater increased with  $\delta^{18}\text{O}$  from D46 to D15, which may have been due to evaporation along the groundwater flow path [35,39]. On the contrary, the  $^{87}\text{Sr}/^{86}\text{Sr}$  ratio approximately decreased with  $\delta^{18}\text{O}$  from D37 to D55 in the Cretaceous aquifer, and the groundwater chemistry was controlled by water–rock interactions [37,45].

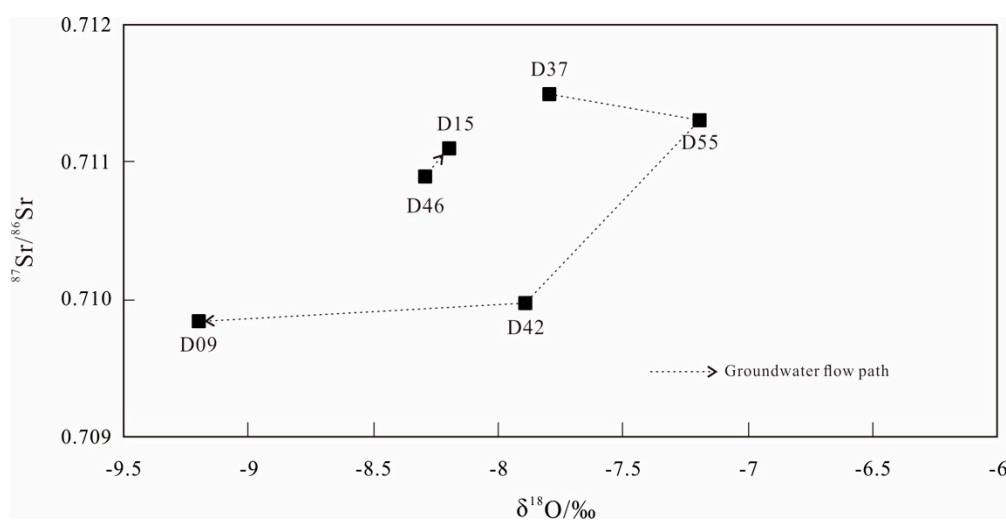
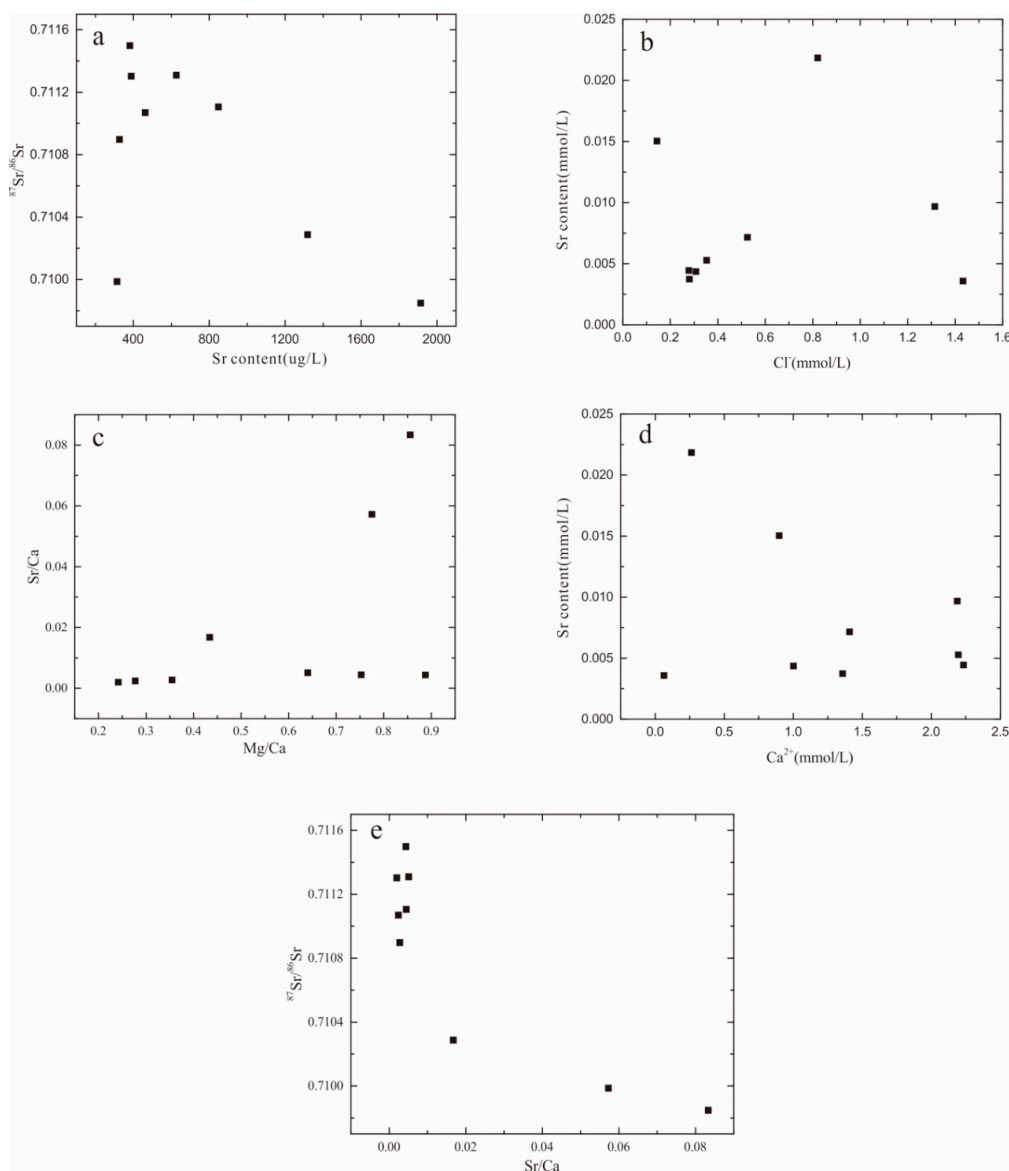


Figure 6. Plot of the  $^{87}\text{Sr}/^{86}\text{Sr}$  ratio versus  $\delta^{18}\text{O}$ .

Moreover, the  $^{87}\text{Sr}/^{86}\text{Sr}$  ratio of the lake-bottom sediments in the two sections ranged from 0.712705 to 0.715187; these values were smaller than those of weathering silicate (0.716–0.720) and greater than that of weathering carbonate (0.708). Yokoo (2004) found that the  $^{87}\text{Sr}/^{86}\text{Sr}$  ratios of evaporite, carbonate, and silicate minerals were 0.71269, 0.71281, and 0.7141, respectively, by using the continuous extraction of sand minerals in loess plateaus and dune deserts [46]. A mineral isotope analysis of a similar area showed that bottom sediments containing strontium east of HL were mainly evaporite and carbonate minerals, and those west of HL were silicate minerals. Moreover, the T2 and T4 samples from northeast of HL had higher strontium concentrations (530 and 450  $\mu\text{g}/\text{g}$ , respectively) than the other samples. The lower  $^{87}\text{Sr}/^{86}\text{Sr}$  ratios were close to those of the bottom sediments of Dakebo Lake [47] and were similar to those of the matrixes of Cretaceous aquifers, such as in the Huanhe Formation [44].

#### 4.5.2. Sr Isotope Characterization in Groundwater

In the study area, there was a large spatial difference in the dissolution characteristics of strontium and in the  $^{87}\text{Sr}/^{86}\text{Sr}$  ratio in the groundwater (Table A1); these values were 314–1914 and 0.709848–0.711498  $\mu\text{g}/\text{L}$ , respectively. The depths of groundwater for the D01 and D20 samples were 15.04 and 19.40 m, respectively. Their strontium concentrations were greater than 1000  $\mu\text{g}/\text{L}$ , and their  $^{87}\text{Sr}/^{86}\text{Sr}$  ratios were 0.709848 and 0.710288, respectively. The D37 sample had a lower strontium concentration of 382  $\mu\text{g}/\text{L}$  and a higher  $^{87}\text{Sr}/^{86}\text{Sr}$  ratio of 0.711498, with a depth of 24.97 m. As shown in Figure 7a, the strontium concentrations were negatively correlated with the  $^{87}\text{Sr}/^{86}\text{Sr}$  ratios in the groundwater, and this relationship was similar to that of the matrix of the aquifers. In general, the  $^{87}\text{Sr}/^{86}\text{Sr}$  ratio of the groundwater depended on that of the soluble minerals in water-bearing media [48]. In the study area, the  $^{87}\text{Sr}/^{86}\text{Sr}$  ratio of the groundwater was higher when the source of strontium was from carbonate and sulfate minerals and from silicate minerals, which were important strontium-bearing minerals in the matrix of the aquifers. The hydrochemical formation of groundwater was controlled by silicate, carbonate, and sulfate leaching.



**Figure 7.** Relationships among Sr concentrations, Sr isotopes, and other ion concentrations of groundwater (a–e).

Studies have shown that the strontium concentrations of rainfall were lower (0.002~0.3 mg/L) than that of groundwater [49,50]. There was a positive relationship between the strontium concentrations and  $\text{Cl}^-$  concentrations for five groundwater samples, as shown in the left bottom of Figure 7b, indicating that the strontium concentrations of the groundwater may have been affected by evaporation. On the other hand, carbonate had lower K and higher Ca mineral concentrations than other rock types and could be rapidly dissolved in groundwater; it had a higher strontium concentrations and a lower  $^{87}\text{Sr}/^{86}\text{Sr}$  ratio than the other rock types [43,47]. As shown in Figure 7d, there was no significant relationship between  $\text{Ca}^{2+}$  and strontium concentrations, and the  $^{87}\text{Sr}/^{86}\text{Sr}$  ratio gradually decreased as the mole ratio of Sr/Ca increased (Figure 7e). The ratio was gradually close to that of carbonate minerals, suggesting that the dissolution of carbonate minerals was not significant in the water–rock interactions.

Moreover, the higher mole ratios of Mg/Ca and Sr/Ca in the groundwater revealed that the dissolution of carbonate minerals was inconsistent (Figure 7c). The increased concentrations of  $\text{Mg}^{2+}$  and  $\text{Sr}^{2+}$  may have been due to dolomite gradually dissolving in the groundwater during calcite precipitation. However, the Sr concentrations were not significantly correlated with the concentration of  $\text{SO}_4^{2-}$  (Figure 8a), and the  $^{87}\text{Sr}/^{86}\text{Sr}$  ratio tended to decrease with increasing  $\text{SO}_4^{2-}$  concentrations (Figure 8b). The  $^{87}\text{Sr}/^{86}\text{Sr}$  ratios of the D42 and D09 samples of 0.709986 and 0.709848, respectively, were close to that of sulfate minerals (0.708), indicating that sulfate minerals may have been dissolved in the groundwater.

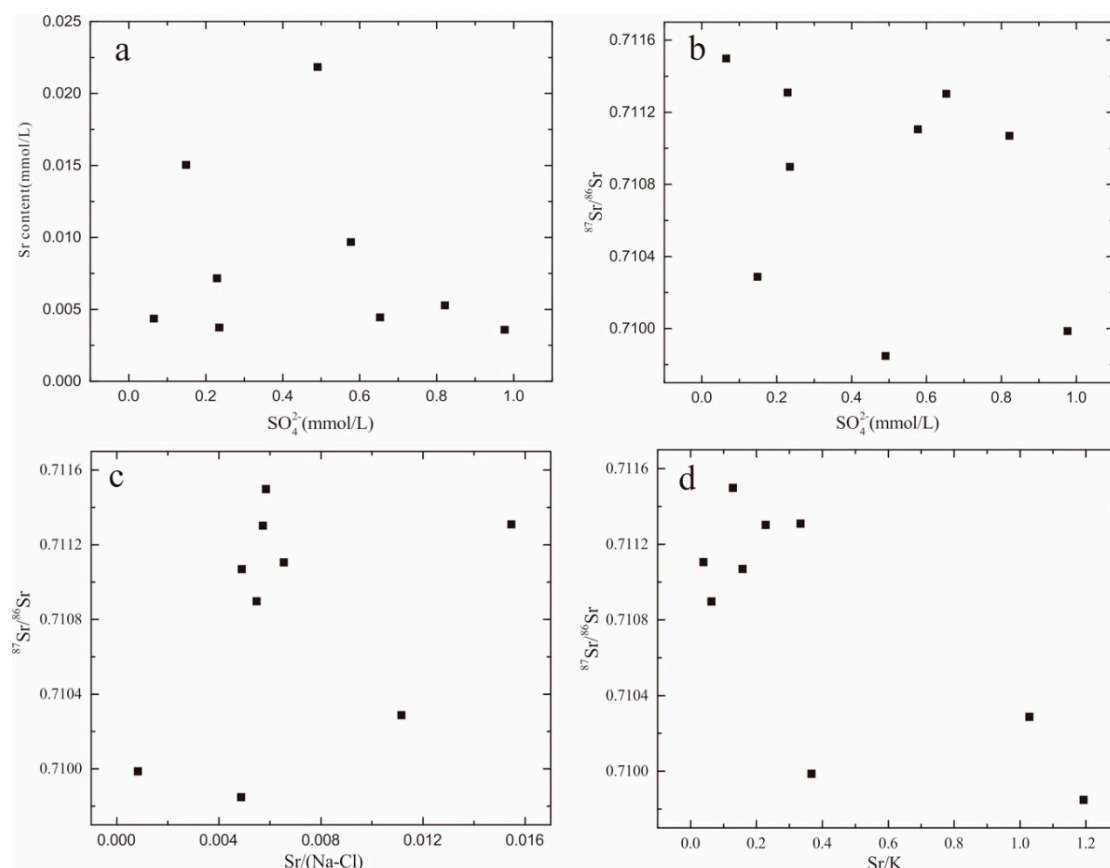


**Figure 8.** Relationships between Sr isotopes and molar ratios between Sr and other ions of groundwater (a–d).

The relationship between the mole ratio of Sr/Ca and the  $^{87}\text{Sr}/^{86}\text{Sr}$  ratio indicated that silicate minerals were dissolved in the groundwater (Figure 7e), i.e., there was a lower mole ratio of Sr/Ca associated with a higher  $^{87}\text{Sr}/^{86}\text{Sr}$  ratio. The  $^{87}\text{Sr}/^{86}\text{Sr}$  value was not significantly correlated with the mole ratio of Sr/(Na–Cl) or with the mole ratio of Sr/K (Figure 8c,d). When the  $^{87}\text{Sr}/^{86}\text{Sr}$  ratio was

higher and the mole ratios of Sr/(Na+Cl) and Sr/K were relatively lower, it may have been due to K-feldspar and albite dissolved in the groundwater.

Su et al. (2011) analyzed the evolution mechanism of the strontium isotope in Cretaceous groundwater in the Ordos Basin and found a higher  $^{87}\text{Sr}/^{86}\text{Sr}$  ratio in K-feldspar (0.728059 and 0.723281) and in albite (0.712973 and 0.713064) [24]. In general, albite was found to dissolve in groundwater more easily than K-feldspar [51]. In the study area, the  $^{87}\text{Sr}/^{86}\text{Sr}$  values were relatively close to those of albite, suggesting that the  $^{87}\text{Sr}/^{86}\text{Sr}$  ratios of groundwater were more affected by the dissolution of albite. Edmunds et al. (2006) found that the  $^{87}\text{Sr}/^{86}\text{Sr}$  ratios of rainfall were 0.71097–0.711682 and that lower Sr concentrations ranged from 0.011 to 0.079  $\mu\text{g}/\text{L}$ , according to investigations of hydrogeochemical evolution and groundwater recharge in the Minqin Basin, Northwest China [52]. The  $^{87}\text{Sr}/^{86}\text{Sr}$  ratios of most of the lake water samples and groundwater samples were smaller than those of the rainfall (Figure 9). The  $^{87}\text{Sr}/^{86}\text{Sr}$  ratios of the D37, D12, and D55 samples were close to the average values of the rainfall, suggesting that the groundwater may have been recharged by rainfall. Moreover, the  $^{87}\text{Sr}/^{86}\text{Sr}$  ratios of the groundwater ranged from those of silicate minerals to those of carbonate and sulfate minerals, indicating that hydrochemical formation was affected by silicate, carbonate, and sulfate minerals.

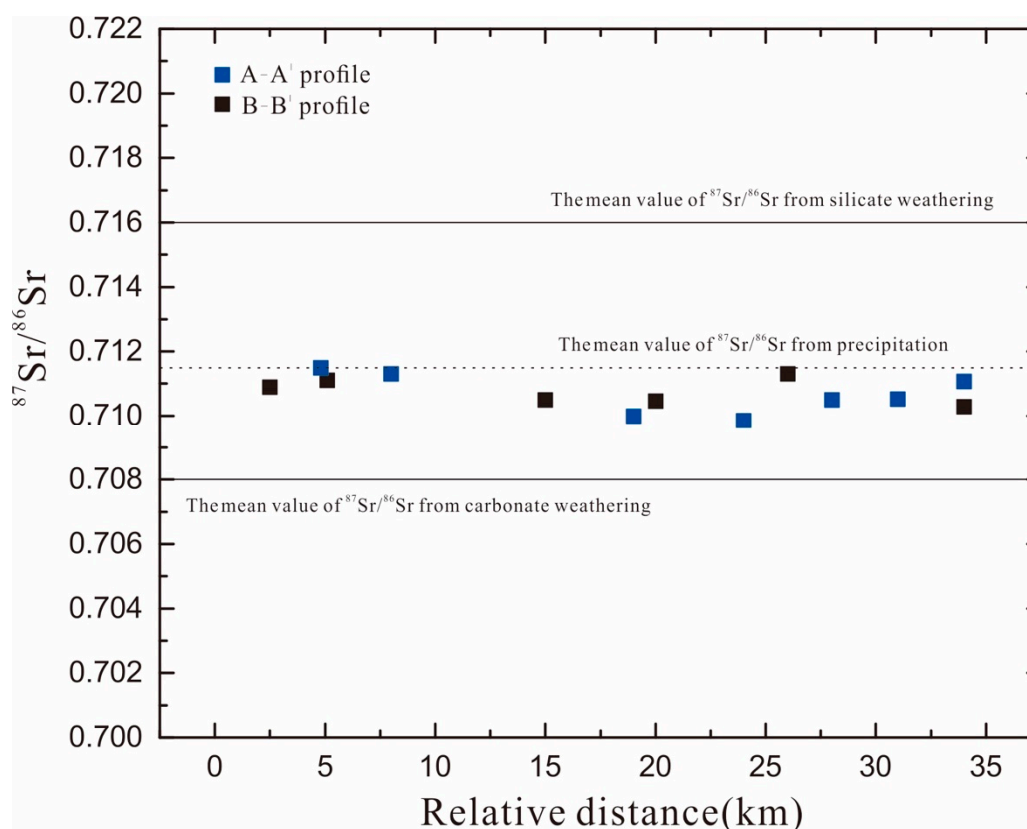


Figure 9.  $^{87}\text{Sr}/^{86}\text{Sr}$  ratio from different sources—lake water and groundwater.

## 5. Conclusions

In this study, hydrochemical parameters, stable hydrogen and oxygen isotopes, and strontium isotopes were used to investigate hydrogeochemical characteristics and their change along the groundwater flow path. Based on the hydrogeochemical characteristics of groundwater, we could evaluate the groundwater quality and study the relationship between groundwater and HL for the sustainable use of water resources. We obtained the following main conclusions from this study:

(1) The major cations of the groundwater were  $\text{Ca}^{2+}$  and  $\text{Na}^{+}$ , the major anion was  $\text{HCO}_3^{-}$ , and the hydrochemical facies were the  $\text{HCO}_3\text{-Ca}$ ,  $\text{HCO}_3\text{-Na}$ , and  $\text{HCO}_3\text{-Ca-Na}$  types. Cation

exchange changed the cation component of the hydrochemical facies along the groundwater flow path. The groundwater samples came from the edge of HB with lower concentration of TDS, which increased and then decreased along the groundwater flow path. Closest to the lakeshore, groundwater became fresher because of mixing due to the convergence of flows from Cretaceous groundwater flow paths.

(2) The hydrochemical parameters and stable isotopes revealed that the hydrochemical formation of the groundwater was mainly affected by water–rock interactions, as well as by evaporation in shallow groundwater areas. The Sr isotope showed that the hydrochemical formation of the groundwater was controlled by silicate leaching. On the basis of an isotope analysis, we found that water–rock interactions and  $\delta^{18}\text{O}$  enrichment caused groundwater samples to deviate from the GMWL and LMWL. Hongjiannao Lake water had heavier isotopes, because open water was affected by intensive evaporation.

**Author Contributions:** Conceptualization, C.W. and X.W.; data curation, C.W., X.W., and W.M.; formal analysis, C.W., W.M., and G.Z.; funding acquisition, X.W.; investigation, C.W., W.M., and X.W.; methodology, C.W. and X.W.; project administration, C.W. and X.W.; resources, C.W.; software, C.W. and G.Z.; supervision, C.W. and X.W.; validation, C.W.; visualization, C.W. and X.W.; writing—original draft, C.W.; writing—review and editing, C.W. and X.W. All authors have read and agreed to the published version of the manuscript.

**Funding:** This research was supported by the National Natural Science Foundation of China (41972259 and 41572227), National Key R&D Program of China (No. 2018YFC0406400).

**Conflicts of Interest:** The authors declare no conflict of interest.

## Appendix A

**Table A1.** Statistical summary for the hydrochemical parameters and isotopes of water samples (sample locations shown in Figure 3).

Sample	Na <sup>+</sup>	K <sup>+</sup>	Mg <sup>2+</sup>	Ca <sup>2+</sup>	Cl <sup>-</sup>	NO <sub>3</sub> <sup>-</sup>	SO <sub>4</sub> <sup>2-</sup>	HCO <sub>3</sub> <sup>-</sup>	CO <sub>3</sub> <sup>2-</sup>	TDS	pH	δD	δ <sup>18</sup> O	<sup>87</sup> Sr/ <sup>86</sup> Sr	Sr <sup>2+</sup>
	mg/L														μg/L
D46	22.1	2.31	11.7	54.4	9.92	20	22.6	236	0	380	7.38	-62.9	-8.3	0.710897	327
D15	64.2	9.73	40	87.7	46.6	2.12	55.4	481	0	787	7.59	-62.3	-8.2	0.711106	848
D04	10.1	1.55	10.1	49.3	4.98	3.71	23.5	182	0	285	8.05	-57.7	-7.7	/	/
D12	24.2	0.76	13.1	89.5	9.85	26.2	62.7	277	0	503	7.34	-71	-8.8	0.711303	389
D23	152	0.95	11.4	67.1	89.1	48.4	112	301	0	782	7.63	-80.6	-10.6	/	/
D20	34.3	0.57	9.47	36	5.08	28.5	14.3	192	0	320	7.66	-62.8	-6.6	0.710288	1318
D30	2308	43.8	78.1	7.53	1929	13.8	670	1402	536	6991	9.14	-26.6	-3.4	0.710491	281
D34	2336	44.4	80.6	6.88	1981	13.8	679	1439	544	7129	9.5	-25.4	-3.2	0.710454	273
D37	24.2	1.33	21.6	40.1	10.9	0.69	6.26	252	6.29	364	8.25	-61.6	-7.8	0.711498	382
D55	22.7	0.84	21.9	56.4	18.6	48.5	22	231	0	422	7.82	-66.2	-7.2	0.71131	627
D42	132	0.38	1.18	2.51	50.8	8.57	93.8	198	11	498	8.84	-63.7	-7.9	0.709986	314
D26	55.9	0.59	15.7	55.4	21.1	77.8	30.6	247	0	505	7.67	-71.5	-8.6	/	/
D09	122	0.72	5.45	10.5	29.1	10.7	47.1	261	0	487	8.03	-78.1	-9.2	0.709848	1914
D01	32.9	1.31	14.8	88	12.5	37	78.9	270	0	536	7.83	-61.3	-7.2	0.711069	463
D28	2323	48.4	80.6	6.88	1967	13.8	677	1406	563	7090	9.16	-28.4	-3.8	0.710522	291
D32	2305	44.3	79.3	5.61	1942	13.8	673	1406	551	7023	9.18	-27	-3.2	0.710491	307

## References

1. Wu, C.; Wu, X.; Qian, C.; Zhu, G. Hydrogeochemistry and groundwater quality assessment of high fluoride levels in the Yanchi endorheic region, northwest China. *Appl. Geochem.* **2018**, *98*, 404–417. [[CrossRef](#)]
2. Yan, B.; Chen, L. Coincidence probability of precipitation for the middle route of south-to-north water transfer project in China. *J. Hydrol.* **2013**, *499*, 19–26. [[CrossRef](#)]
3. Lin, J.; Ma, R.; Hu, Y.; Sun, Z.; Wang, Y.; McCarter, C. Groundwater sustainability and groundwater/surface-water interaction in arid Dunhuang Basin, northwest China. *Hydrogeol. J.* **2018**, *26*, 1559–1572. [[CrossRef](#)]
4. Li, Y.; Hu, F.; Xue, Z.; Yu, Y.; Wu, P. Hydrogeochemical and isotopic characteristics of groundwater in the salt chemical industrial base of Guyuan City, northwestern China. *Arab. J. Geosci.* **2014**, *8*, 3427–3440. [[CrossRef](#)]
5. Qian, C.; Wu, X.; Mu, W.; Fu, R.; Zhu, G.; Wang, Z.; Wang, D. Hydrogeochemical characterization and suitability assessment of groundwater in an agro-pastoral area, Ordos Basin, NW China. *Environ. Earth Sci.* **2016**, *75*, 1356. [[CrossRef](#)]
6. Huang, X.; Wang, G.; Liang, X.; Cui, L. Hydrochemical and stable isotope ( $\delta D$  and  $\delta^{18}O$ ) characteristics of groundwater and hydrogeochemical processes in the Ningtiaota Coalfield, Northwest China. *Mine Water Environ.* **2018**, *37*, 119–136. [[CrossRef](#)]
7. Zhou, Z.; Wang, J.; Su, R.; Guo, Y.; Zhao, J.; Zhang, M.; Ji, R.; Li, Y.; Li, J. Hydrogeochemical and isotopic characteristics of groundwater in Xinchang preselected site and their implications. *Environ. Sci. Pollut. Res.* **2019**. [[CrossRef](#)]
8. Rusi, S.; Di Curzio, D.; Palmucci, W.; Petaccia, R. Detection of the natural origin hydrocarbon contamination in carbonate aquifers (central Apennine, Italy). *Environ. Sci. Pollut. Res.* **2018**, *25*, 15577–15596. [[CrossRef](#)]
9. Gomo, M.; Vermeulen, D. Hydrogeochemical characteristics of a flooded underground coal mine groundwater system. *J. Afr. Earth Sci.* **2014**, *92*, 68–75. [[CrossRef](#)]
10. Ersoy, A.; Sönmez, S. Hydrogeochemical and isotopic characteristics of the Ilica geothermal system (Erzurum, Turkey). *Environ. Earth Sci.* **2014**, *72*, 4451–4462. [[CrossRef](#)]
11. Bozdogan, A. Hydrogeochemical and isotopic characteristics of Kavak (Seydisehir-Konya) geothermal field, Turkey. *J. Afr. Earth Sci.* **2016**, *121*, 72–83. [[CrossRef](#)]
12. Ako, A.; Shimada, J.; Hosono, T.; Ichianagi, K.; Nkeng, G.; Eyong, G.; Roger, N. Hydrogeochemical and isotopic characteristics of groundwater in Mbanga, Njombe and Penja (Banana Plain)-Cameroon. *J. Afr. Earth Sci.* **2012**, *75*, 25–36. [[CrossRef](#)]
13. Liang, K. Quantifying streamflow variations in ungauged lake basins by integrating remote sensing and water balance modelling: A case study of the erdos larus relictus national nature reserve, China. *Remote Sens.* **2017**, *9*, 588. [[CrossRef](#)]
14. Liang, K.; Yan, G. Application of landsat imagery to investigate lake area variations and relict gull habitat in hongjian lake, Ordos Plateau, China. *Remote Sens.* **2017**, *9*, 1019. [[CrossRef](#)]
15. Shen, J.; Wang, Y.; Yang, X.; Zhang, E.; Yang, B.; Ji, J. Paleosandstorm characteristics and lake evolution history deduced from investigation on lacustrine sediments-The case of Hongjiannao Lake, Shaanxi Province. *Chin. Sci. Bull.* **2005**, *50*, 2355–2361.
16. Wang, Y.; Yan, Z.; Gao, F. Monitoring spatio-temporal changes of water area in Hongjiannao Lake from 1957 to 2015 and its driving forces analysis. *Trans. Chin. Soc. Agric. Eng.* **2018**, *34*, 265–271.
17. Jiang, X.; Wan, L.; Wang, X.; Wang, D.; Wang, H.; Zhang, J.; Zhang, H.; Zhao, Z.; Yu, K. A multi-method study of regional groundwater circulation in the Ordos Plateau, NW China. *Hydrogeol. J.* **2018**, *26*, 1657–1668. [[CrossRef](#)]
18. Hou, G.; Zhang, M.; Liu, F.; Wang, Y.; Liang, Y. *Groundwater Investigation in the Ordos Basin*; Geological Publishing House: Beijing, China, 2008; pp. 39–48.
19. Liotta, M.; Alessandro, W.; Arienzo, I.; Longo, M. Tracing the circulation of groundwater in volcanic systems using the  $^{87}Sr/^{86}Sr$  ratio: Application to Mt. Etna. *J. Volcanol. Geotherm. Res.* **2017**, *331*, 102–107. [[CrossRef](#)]
20. Dou, Y.; Hou, G.; Qian, H. Groundwater circulation by hydrochemistry and isotope method. In *Water Resources Environment*; CRC Press: Boca Raton, FL, USA, 2016; pp. 13–16.
21. Awaleh, M.; Baudron, P.; Soubaneh, Y.; Boschetti, T.; Hoch, F.; Egueh, N.; Mohamed, J.; Dabar, O.; Masse-Dufresne, J.; Gassani, J. Recharge, groundwater flow pattern and contamination processes in an arid volcanic area: Insights from isotopic and geochemical tracers (Bara aquifer system, Republic of Djibouti). *J. Geochem. Explor.* **2017**, *175*, 82–98. [[CrossRef](#)]

22. Asante, J.; Dotson, S.; Hart, E.; Kreamer, D. Water circulation in karst systems: Comparing physicochemical and environmental isotopic data interpretation. *Environ. Earth Sci.* **2018**, *77*, 421. [[CrossRef](#)]
23. Calligaris, C.; Mezga, K.; Slejko, F.; Urbanc, J.; Zini, L. Groundwater characterization by means of conservative ( $\delta^{18}\text{O}$  and  $\delta^2\text{H}$ ) and non-Conservative ( $^{87}\text{Sr}/^{86}\text{Sr}$ ) isotopic values: The classical Karst region aquifer case (Italy-Slovenia). *Geosci. J.* **2018**, *8*, 321. [[CrossRef](#)]
24. Su, X.; Wu, C.; Dong, W.; Hou, G. Strontium isotope evolution mechanism of the Cretaceous groundwater in Ordos Desert Plateau. *J. Chendu Univ. Technol.* **2011**, *3*, 348–358.
25. Palmucci, W.; Rusi, S.; Pennisi, M.; Curzio, D. Contribution of B and Sr Isotopes to assess boron contamination of groundwater: Case studies in Central Italy. *Rend. Online Soc. Geol. Ital.* **2016**, *41*, 65–68. [[CrossRef](#)]
26. Dansgaard, W. Stable isotopes in precipitation. *Tellus* **1964**, *16*, 436–468. [[CrossRef](#)]
27. Schoeller, H. Geochemistry of groundwater. In *Groundwater Studies-an International Guide for Research and Practice*; UNESCO: Paris, France, 1984; pp. 1–46.
28. Cui, J.; Tian, L.; Biggs, T.; Rong, W. Deuterium-excess determination of evaporation to inflow ratios of an alpine lake: Implications for water balance and modeling. *Hydrol. Process.* **2017**, *31*, 1034–1046. [[CrossRef](#)]
29. Zhou, X.; Jin, X.; Liang, S.; Shen, Y.; Zhang, H. *Groundwater Science Monograph*; Geological Publishing House: Beijing, China, 2010; pp. 34–50.
30. Clark, I.; Fritz, P. *Environmental Isotope in Hydrogeology*; Lewis Publishers: New York, NY, USA, 1997; pp. 58–72.
31. Hu, Y.; Liu, Z.; Zhao, M.; Zeng, Q.; Zeng, C.; Chen, B.; Chen, C.; He, H.; Cai, X.; Ou, Y.; et al. Using deuterium excess, precipitation and runoff data to determine evaporation and transpiration: A case study from the Shawan Test Site, Puding, Guizhou, China. *Geochim. Cosmochim. Acta* **2018**, *242*, 21–33. [[CrossRef](#)]
32. Li, P.; Wu, J.; Qian, H.; Zhang, Y.; Yang, N.; Jing, L.; Yu, P. Hydrogeochemical characterization of groundwater in and around a wastewater irrigated forest in the southeastern edge of the Tengger Desert, Northwest China. *Expo. Health* **2016**, *8*, 331–348. [[CrossRef](#)]
33. Liu, J.; Guo, H.; Liu, F.; Wei, W.; Zhang, L.; Zhang, X. The variations of stable isotopes ( $\delta\text{D}$  and  $\delta^{18}\text{O}$ ) in the precipitation in Baotou area. *J. Arid Land Resour. Environ.* **2013**, *5*, 157–162.
34. Kim, K.; Lee, X. Isotopic enrichment of liquid water during evaporation from water surfaces. *J. Hydrol.* **2011**, *399*, 364–375. [[CrossRef](#)]
35. Amiri, V.; Nakhaei, M.; Lak, R.; Kholghi, M. Geophysical, isotopic, and hydrogeochemical tools to identify potential impacts on coastal groundwater resources from Urmia hypersaline Lake, NW Iran. *Environ. Sci. Pollut. Res.* **2016**, *23*, 16738–16760. [[CrossRef](#)] [[PubMed](#)]
36. Wang, M.; Zhou, X.; Wang, J.; Li, X.; Liu, H. Occurrence, genesis and travertine deposition of the Adong hot springs in northwestern Yunnan of China. *Geothermics* **2020**. [[CrossRef](#)]
37. Ettayfi, N.; Bouchaou, L.; Michelot, J.; Tagma, T.; Warner, N.; Boutaleb, S.; Massault, M.; Lgourna, Z.; Vengosh, A. Geochemical and isotopic (oxygen, hydrogen, carbon, strontium) constraints for the origin, salinity, and residence time of groundwater from a carbonate aquifer in the Western Anti-Atlas Mountains, Morocco. *J. Hydrol.* **2012**, *438–439*, 97–111. [[CrossRef](#)]
38. Sahib, L.; Marandi, A.; Schüth, C. Strontium isotopes as an indicator for groundwater salinity sources in the Kirkuk region, Iraq. *Sci. Total Environ.* **2016**, *562*, 935–945. [[CrossRef](#)] [[PubMed](#)]
39. Lu, L.; Pang, Z.; Kong, Y.; Wang, Y.; Guo, Q.; Gu, W.; Zhou, L.; Yu, D.; Xu, C. Geochemical and isotopic evidence on the recharge and circulation of geothermal water in the Tangshan Geothermal System near Nanjing, China: Implications for sustainable development. *Hydrogeol. J.* **2018**, *26*, 1705–1719. [[CrossRef](#)]
40. Peterman, Z.; Thamke, J.; Futa, K.; Preston, T. Strontium isotope systematics of mixing groundwater and oil-field brine at Goose Lake in northeastern Montana, USA. *Appl. Geochem.* **2012**, *27*, 2403–2408. [[CrossRef](#)]
41. Jiang, Y. Strontium isotope geochemistry of groundwater affected by human activities in Nandong underground river system, China. *Appl. Geochem.* **2011**, *26*, 371–379. [[CrossRef](#)]
42. Xie, X.; Wang, Y.; Ellis, A.; Su, C.; Li, J.; Li, M.; Duan, M. Delineation of groundwater flow paths using hydrochemical and strontium isotope composition: A case study in high arsenic aquifer systems of the Datong basin, northern China. *J. Hydrol.* **2013**, *476*, 87–96. [[CrossRef](#)]
43. Bakari, S.; Aagaard, P.; Vogt, R.; Ruden, F.; Johansen, I.; Vuai, S. Strontium isotopes as tracers for quantifying mixing of groundwater in the alluvial plain of a coastal watershed, south-eastern Tanzania. *J. Geochem. Explor.* **2013**, *130*, 1–14. [[CrossRef](#)]

44. Rao, W.; Jin, K.; Jiang, S.; Tan, H.; Han, L.; Tang, Q. Chemical and strontium isotopic characteristics of shallow groundwater in the Ordos Desert Plateau, North China: Implications for the dissolved sr source and water-rock interactions. *Geochemistry* **2015**, *75*, 365–374. [[CrossRef](#)]
45. Uliana, M.; Banner, J.; Sharp, J. Regional groundwater flow paths in Trans-Pecos, Texas inferred from oxygen, hydrogen, and strontium isotopes. *J. Hydrol.* **2007**, *334*, 334–346. [[CrossRef](#)]
46. Yokoo, Y.; Nakano, T.; Nishikawa, M.; Hao, Q. Mineralogical variation of Sr-Nd isotopic and elemental compositions in loess and desert sand from the central loess plateau in China as a provenance tracer of wet and dry deposition in the northwestern Pacific. *Chem. Geol.* **2004**, *204*, 45–62. [[CrossRef](#)]
47. Yang, Y.; Hou, G.; Zhao, Z.; Tao, Z.; Yin, L.; Wang, D.; Su, X. Formation of mud springs in the Cretaceous Ordos groundwater basin, China and their hydrogeological significance. *Geol. Bull. China* **2008**, *27*, 1173–1177.
48. Dotsika, E.; Poutoukis, D.; Kloppmann, W.; Guerrot, C.; Voutsas, D.; Kouimtzis, T. The use of O, H, B, Sr and S isotopes for tracing the origin of dissolved boron in groundwater in Central Macedonia, Greece. *Appl. Geochem.* **2010**, *25*, 1783–1796. [[CrossRef](#)]
49. Bullen, T.; Krabbenhoft, D.; Kendall, C. Kinetic and mineralogic controls on the evolution of groundwater chemistry and  $^{87}\text{sr}/^{86}\text{sr}$  in a sandy silicate aquifer, northern Wisconsin, USA. *Geochim. Cosmochim. Acta* **1996**, *60*, 1807–1821. [[CrossRef](#)]
50. Négrel, P.; Petelet-Giraud, E. Strontium isotopes as tracers of groundwater-induced floods: The Somme case study (France). *J. Hydrol.* **2005**, *305*, 99–119. [[CrossRef](#)]
51. Lasaga, A. Chemical kinetics of water-rock interactions. *J. Geophys. Res.* **1974**, *89*, 4009–4025. [[CrossRef](#)]
52. Edmunds, W.; Ma, J.; Aeschbach-Hertig, W.; Kipfer, R.; Darbyshire, D. Groundwater recharge history and hydrogeochemical evolution in the Minqin Basin, North West China. *Appl. Geochem.* **2006**, *21*, 2148–2170. [[CrossRef](#)]



© 2020 by the authors. Licensee MDPI, Basel, Switzerland. This article is an open access article distributed under the terms and conditions of the Creative Commons Attribution (CC BY) license (<http://creativecommons.org/licenses/by/4.0/>).